

Research Article

Open Access



# One-pot synthesis of carbon dots/hydrochar and visible-light-driven photocatalysts for aerobic oxidative coupling of benzylic amines

Xihua Cao<sup>1,2,3,4,5,#</sup>, Yi Zhao<sup>1,2,3,4,5,#</sup>, Junyang Leng<sup>1,2,3,4,5</sup>, Xiaoli Bai<sup>1,2,3,4,5</sup>, Yining Qu<sup>1,2,3,4,5</sup>, Liang Jiang<sup>1,2,3,4,5</sup>, Daomei Chen<sup>1,2,3,4,5</sup>, Jiaqiang Wang<sup>1,2,3,4,5,\*</sup>

<sup>1</sup>School of Chemical Sciences & Technology, Yunnan University, Kunming 650091, Yunnan, China.

<sup>2</sup>School of Materials and Energy, Yunnan University, Kunming 650091, Yunnan, China.

<sup>3</sup>Yunnan Institute of Frontier Technologies in Water Treatment, Kunming 650091, Yunnan, China.

<sup>4</sup>National Center for International Research on Photoelectric and Energy Materials, Kunming 650091, Yunnan, China.

<sup>5</sup>School of Engineering, Yunnan University, Kunming 650091, Yunnan, China.

#Authors contributed equally.

\*Correspondence to: Prof. Jiaqiang Wang, School of Chemical Sciences & Technology, Yunnan University, 2 Cuihu North Road, Wuhua District, Kunming 650091, Yunnan, China. E-mail: jqwang@ynu.edu.cn

**How to cite this article:** Cao X, Zhao Y, Leng J, Bai X, Qu Y, Jiang L, Chen D, Wang J. One-pot synthesis of carbon dots/hydrochar and visible-light-driven photocatalysts for aerobic oxidative coupling of benzylic amines. *Chem Synth* 2024;4:58. <https://dx.doi.org/10.20517/cs.2024.21>

**Received:** 17 Feb 2024 **First Decision:** 20 Jun 2024 **Revised:** 2 Jul 2024 **Accepted:** 9 Jul 2024 **Published:** 8 Oct 2024

**Academic Editor:** Jin Xie **Copy Editor:** Dong-Li Li **Production Editor:** Dong-Li Li

## Abstract

Utilizing selective photocatalysis conversion of amines represents an environmentally sustainable and economically feasible approach to generating valuable chemical products in the industry. Herein, carbon dots (CDs) incorporated in hydrochar (CDs/HCPP) were synthesized by one-pot hydrothermal carbonization of pomelo peel (PP) coupled with freeze-drying and used for aerobic oxidative coupling of benzylic amines. CDs were produced using only the pomelo peel as the carbon source, without the addition of any extra carbon additives. CDs/HCPP exhibited the greatest catalytic activity, achieving a benzylamine conversion rate of 99%, which was nearly 5.5 times of carbonized PP (CPP) without CDs and 1.14 times of CDs alone. Additionally, the oxidation of other amines, such as *p*-substituted benzylamines with groups that donate and withdraw electrons, was also demonstrated to be highly active and reusable using CDs/HCPP. This study has the potential to pave the way for novel methodologies and insights into synthesizing biomass composites adorned with CDs, enhancing the efficacy of photocatalytic syntheses.

**Keywords:** Carbon dots/hydrochar, metal-free photocatalysts, photocatalytic oxidative coupling of amine, imine



© The Author(s) 2024. **Open Access** This article is licensed under a Creative Commons Attribution 4.0 International License (<https://creativecommons.org/licenses/by/4.0/>), which permits unrestricted use, sharing, adaptation, distribution and reproduction in any medium or format, for any purpose, even commercially, as long as you give appropriate credit to the original author(s) and the source, provide a link to the Creative Commons license, and indicate if changes were made.



## INTRODUCTION

As important components of numerous fine chemicals, pharmaceuticals and molecular motors, the oxidative coupling of benzylamine and imine derivatives has attracted extensive attention. Various catalytic methods have been explored to effectively convert benzylamine to imine counterpart, among which metal-based catalysts have been intensively studied<sup>[1]</sup>. Recent years have seen a few metal-free carbon nanomaterials, such as graphene oxides, doped carbons, and oxygen-rich carbon quantum dots, emerging as cost-effective and sustainable catalysts for amine oxidation<sup>[2]</sup>.

However, despite these promising developments, challenges persist, as the synthesis of these materials often entails intricate procedures, substantial catalyst loading, extended reaction times, and elevated oxygen requirements in the reaction. In contrast, the pursuit of photocatalytic reactions, driven by visible light, has taken center stage. This strategy harnesses sustainable solar energy while minimizing environmental concerns<sup>[3]</sup>.

The scientific community has witnessed a plethora of explorations in this domain, utilizing various systems, including graphitic carbon nitride (g-C<sub>3</sub>N<sub>4</sub>), bipyridine complexes, metal-organic frameworks (MOFs) and C<sub>70</sub> fullerenes, all in pursuit of this transformative goal<sup>[4-9]</sup>.

Carbon dots (CDs) have garnered substantial attention as potent photocatalysts for degrading pollutants, splitting water, and reducing CO<sub>2</sub> owing to their remarkable light-harvesting capabilities, abundant surface defects, active sites, excellent photostability, and good charge separation and transfer capabilities<sup>[10,11]</sup>. Quite recently, CDs have been applied in photocatalytic benzylamine couplings because CDs with hydroxyl and carboxylic groups permit great water solubility, biocompatibility, and exceptional catalytic support and stabilization<sup>[12,13]</sup>. Nevertheless, the limited photostability and chemical stability of CDs in photocatalytic reactions often lead to issues such as aggregation and etching, which restricts their potential applications<sup>[14,15]</sup>. Usually, CDs hybridized with other carbon materials, metals, or metal-based semiconductors to improve durability and synergistically to improve the photocatalytic performance<sup>[16-18]</sup>, their functional photoinduced electron-accepting properties may be attributed to this<sup>[19]</sup>. For example, CDs/Cu<sub>2</sub>O heterogeneous nanocomposite demonstrated enhanced performance in comparison to Cu<sub>2</sub>O alone and CDs when utilized in the photocatalytic coupling of amines<sup>[20]</sup>. The CDs/Bi<sub>2</sub>MoO<sub>6</sub> nanocomposite fabricated by incorporating CDs onto the nanoplates of Bi<sub>2</sub>MoO<sub>6</sub> exhibited enhanced photocatalytic efficacy compared to the pure Bi<sub>2</sub>MoO<sub>6</sub> in the photocatalytic oxidation of amines<sup>[21]</sup>. Notably, even a single cobalt atom catalyst incorporated within CDs has demonstrated exceptional efficiency in amine coupling under visible light irradiation<sup>[22]</sup>. These results unveil the efficacy of introducing CDs in significantly enhancing visible light photocatalytic activity.

Nevertheless, current limited reports focus on the syntheses of CD composites mainly by preparing CDs and their composite components separately<sup>[23-25]</sup>. The practicality of hybrid photocatalysts is limited due to the multi-step preparation process required for this type of method. Moreover, these techniques entail either a complicated catalytic setup or severe reaction conditions<sup>[26]</sup>. Furthermore, additives, such as sucrose<sup>[27]</sup>, citric acid<sup>[28]</sup> and ethylenediamine<sup>[29]</sup>, were often employed in the solvothermal method.

It is worth noting that hydrochar, resulting from the carbonization of biomass with its inherent micro and macro structures, has garnered recognition as a formidable catalyst for amine oxidation<sup>[30,31]</sup>. Lately, an inexpensive hydrochar substance produced through straightforward hydrothermal carbonization of maple and straw demonstrated notable effectiveness (93% yield) in the aerobic oxidation of various amines, employing 0.5 Mpa oxygen as an oxidizing agent in methylbenzene at 373 K<sup>[32]</sup>.

Concerning the manufacture of biochar from forest residues and agricultural wastes, various carbonization techniques were employed, including hydrothermal carbonization, gasification, pyrolysis, and flash carbonization. Over the past decade, hydrothermal carbonization has demonstrated significant potential in biomass conversion to biochar or hydrochar at comparatively lower processing temperatures. This is due to the ability of the hydrothermal process to generate numerous surface oxygenated groups, which subsequently serve as catalytically active sites<sup>[33,34]</sup>. In addition, hydrochar can induce reactive oxygen species (ROS) under light irradiation, such as superoxide anion radical ( $\cdot\text{O}_2^-$ ),  $\text{H}_2\text{O}_2$ , and  $^1\text{O}_2$ <sup>[35,36]</sup>, which exhibit various oxidizing abilities for different substrates<sup>[37,38]</sup>.

The hydrochars derived from biomass have been shown to be effective in diverse organic conversions, such as Knoevenagel, Aldol condensation, and transesterification<sup>[39-41]</sup>. Interestingly, they exhibit oxidative coupling activity towards amines under high temperature and pressure conditions<sup>[32]</sup>. In a recent development, a metal-free hydrochar was synthesized from bamboo specifically for the photocatalytic oxidation of amines to imines. This process was conducted under light in the visible spectrum conditions, employing 0.1 Mpa oxygen as an oxidizer and a 35 W tungsten-halogen lamp as the source of visible illumination, while a very long reaction time (32 h) was required<sup>[42]</sup>.

Pomelo peel (PP) has a three-dimensional porous structure with interconnections with a great quantity of oxygen-containing functional groups, which present promising alternatives for biochar material preparation<sup>[43-45]</sup>. Limited reports so far have concentrated on the utilization of PP for the extraction of aromatic oil<sup>[46]</sup>, fabrication of porous adsorbents<sup>[47,48]</sup>, renewable fuel from biomass<sup>[49]</sup>, solar evaporation<sup>[50-52]</sup>, etc. So far, the photocatalytic application of PP-derived hydrochar has not been explored, let alone the hydrochar incorporated with CDs.

In this study, CDs from PP incorporated in hydrochar (CDs/HCPP) were prepared via one-pot hydrothermal method with freeze-drying without adding any extra carbon additives and the oxidative coupling of benzylamine under aerobic conditions was employed. For comparison, the photocatalytic activities of carbonized PP (CPP) without CDs and CDs alone were also studied. The possible mechanism was proposed.

## EXPERIMENTAL

### General

All chemicals are sourced from commercial suppliers and are suitable for immediate use without additional purification. Additionally, 0.22  $\mu\text{m}$  microporous membrane and dialysis bags (retained molecular weight: 3,500 Da) were purchased from Tianjin Dongkang Technology Co., Ltd (China).

### Pretreatment of PP

Initially, fresh PP was obtained from pomelos peels purchased from a local market in Kunming, Yunnan Province, China. The PP samples were cut into pieces, washed multiple times with deionized water, and left to sun-dry until completely dried. The preparation method of the material is robust and universally applicable.

### Preparation of CPP

PP was calcined at 500, 600, 700, and 800  $^{\circ}\text{C}$  for 4 h with a heating rate of 5  $^{\circ}\text{C}\cdot\text{min}^{-1}$  to obtain CPP, denoted as CPP-x (x = 500, 600, 700, 800).

### Preparation of CDs

In a typical synthesis, a certain amount of PP was added into 60 mL of demineralized water. The mixture is then heated in a 100 mL poly(tetrafluoroethylene) (PTFE)-lined autoclave at 200 °C for 24 h. After the reaction, the reactor is opened after cooling to ambient temperature. After filtering the reaction solution, the liquid is centrifuged for ten minutes at a speed of 12,000 rpm. The resulting brown solution was then filtered through a 0.22 µm microfiltration hydrophilic membranes. After that, the filtrate was dialyzed against deionized water in a dialysis bag (about 3 days), with the water being refreshed periodically (about 12 h). After lyophilization, a brown powder was obtained, which was denoted as CDs.

### Preparation of CDs/HCPP and CDs/HCPP-700

The product collected and freeze-dried from the reaction solution was crushed into powder and denoted as CDs/HCPP (CDs/hydrochar derived from PP). To investigate the structural changes in hydrochar, 3 g CDs/HCPP was further annealed at a heating rate of 5 °C/min to a desired temperature (700 °C) under the protection of N<sub>2</sub> atmosphere and maintained for 4 h. Upon reaching room temperature, the sample was grounded into powder and denoted as CDs/HCPP-700.

### Procedure for the oxidative coupling of amine

Add 5 mL of acetonitrile containing 0.2 mmol of amine to a 20 mL glass vial containing 20 mg photocatalyst. The mixture was stirred for 1 h before photoexcitation. Blue light-emitting diodes (LEDs) (10 W, 460-465 nm) were used as the irradiation source. The intensity of light used for the photocatalyst tests was 795.113 mW/cm<sup>2</sup>. Test report of the light used in the study is added in Sx. After the reaction, the photocatalyst is separated from the mixture using centrifugation. Gas chromatography (GC, Shimadzu GC-2014, DB-5, 30 m × 0.25 mm × 0.25 mm) with a flame ionization detector (FID) and GC-Mass Spectrometry (MS) (Finnigan TRACE DSQ) generated data results that can be used for product analysis and identification.

### Recycling test

The photocatalyst obtained through centrifugation is subjected to five consecutive washes with acetonitrile to remove any residual reactants or by-products. After thorough washing, the catalyst is dried overnight at 90 °C in an oven to remove any solvent and ensure complete dryness. Subsequently, the dried catalyst is directly used in subsequent recycling reactions without further treatment. To evaluate the structural stability of the catalyst, X-ray diffraction (XRD) analysis is conducted.

### Characterization

The elemental composition of samples including C, H, and N was measured using an elemental analyzer (Vario EL III, Elementar, Germany). The textural properties of samples were measured by N<sub>2</sub> adsorption-desorption at 77 K using a Micromeritics ASAP 2460 Surface Area and Porosity Analyzer (Micromeritics, USA). The crystallographic structure was identified by XRD (TTR III, Rigaku, Japan) with Cu K $\alpha$  radiation ( $\lambda = 1.542 \text{ \AA}$ ). The surface electronic states were examined by X-ray photoelectron spectroscopy (XPS, K-Alpha+, Thermo Fisher, USA) with Al K $\alpha$  radiation. The surface morphology was characterized using transmission electron microscopy (TEM, JEM-2100, JEOL, Japan) and scanning electron microscopy (SEM, Quanta 200 FEG, FEI, USA). Raman spectra were collected using a RenishawinVia spectrometer (Renishaw, UK). The surface functional groups were determined using Fourier transform infrared spectroscopy (FT-IR, Nicolet iS10, Thermo Fisher, USA). To examine the formation of radical species in the reaction system, electron paramagnetic resonance (EPR) spectra were gathered at ambient temperature using a Bruker EMX nano spectrometer.

## RESULTS AND DISCUSSION

### Synthesis of CPP, CDs, CDs/HCPP and CDs/CPP

Figure 1 describes the comparison for the synthesis of hydrochar incorporated CDs between our methods and those in the literature. It is a well-established fact that the sole carbonization process (illustrated as the red line in route 1 in Figure 1) does not yield CDs. Consequently, supplementary must be introduced to generate CDs or their composites (route 1 in Figure 1). Moreover, the majority of studies focusing on the fabrication of CDs through hydrothermal treatment have concentrated on creating CDs from the suspension of hydrothermal products (as delineated in route 2 in Figure 1), often overlooking the presence of hydrochar in the process.

By chance, by employing freeze-drying after hydrothermal carbonization of PP, a great number of CDs were found embedded on the hydrochar (solid product after hydrothermal reaction) (route 3 in Figure 1). As illustrated below, the dark brown sample, denoted as CDs/HCPP, was obtained from the hydrothermal treatment of PP. For comparison, the CPP obtained at a pyrolysis temperature of 700 °C was dispersed in the suspension of CDs under vigorous stirring for 24 h, which is denoted as CDs/CPP.

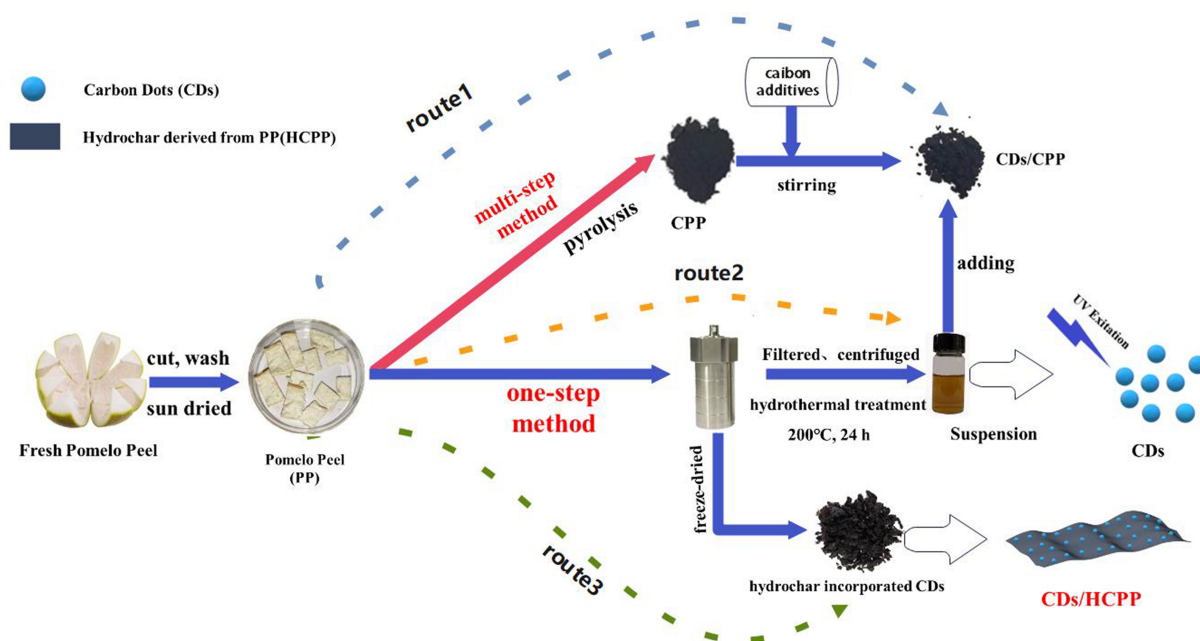
### Characterization of CDs and CDs/HCPP

The XRD test results can characterize the composition and crystal structure of the material, as shown in Figure 2, which shows the XRD patterns of PP, CDs, CDs/HCPP and CDs/HCPP-700. A broad and wide diffraction peak in the range of  $2\theta$  values from  $18^\circ$  to  $28^\circ$  was detected in the catalysts, confirming the presence of the (002) phase of the graphitic domain<sup>[53]</sup>. This peak indicates the formation of a limited number of graphitic phases in the biomass carbon during the calcination process. Compared to the standard XRD patterns of CDs and PP, the XRD patterns of CDs/HCPP composite materials are highly consistent with them. CDs/HCPP-700 and CPP contain a higher proportion of amorphous carbon structures and partially graphitized carbon structures, which are formed during their pyrolytic carbonization process [Supplementary Figure 1].

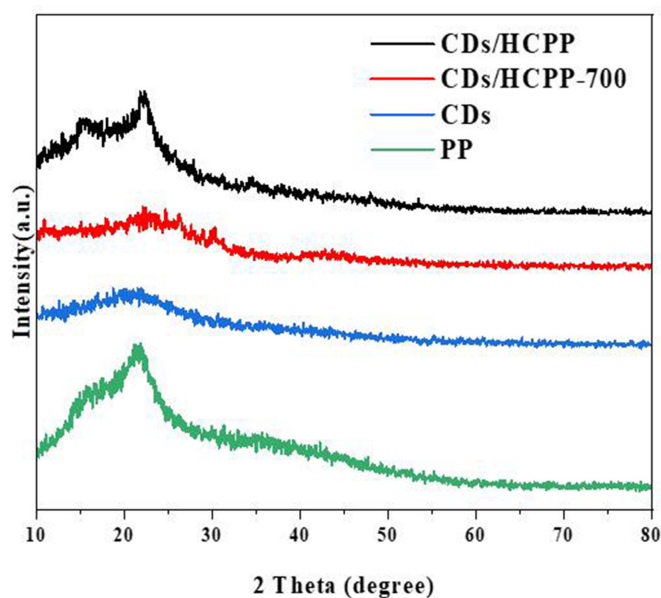
During  $N_2$  adsorption/desorption experiments, PP, CDs/HCPP, and CDs/HCPP-700 displayed an IV-type isotherm featuring a distinct hysteresis loop [Supplementary Figure 2], indicating a highly porous structure. In Supplementary Figure 2, it is evident that the PP and CDs/HCPP-700 samples show almost negligible pore volume on their outer surface, implying a sparse microporous structure that could potentially influence their performance in specific applications. In contrast, the CDs/HCPP sample prepared via a one-step hydrothermal method exhibits significant pore volume within a smaller pore size range. As pore size increases, the pore volume decreases rapidly, indicating abundant microporous structures in both materials, which are advantageous for enhancing adsorption capacity and catalytic efficiency. The Brunauer-Emmett-Teller (BET) surface area of CDs/HCPP ( $16.0 \text{ m}^2/\text{g}$ ) and CDs/HCPP-700 ( $4.2 \text{ m}^2/\text{g}$ ) exhibits a relatively higher surface area compared to the untreated material ( $3.6 \text{ m}^2/\text{g}$ ), which can serve to expose more active sites as a supplement.

The XPS measurement results can serve as the basis for analyzing the elemental composition of the samples. Figure 3A shows the main elemental composition of the sample, including C, N, and O. The outcomes of the quantitative analysis are delineated in Supplementary Table 1. The elemental analysis results indicate that hydrothermal treatment resulted in a slight decrease in the oxygen content of the samples [Supplementary Table 2].

Three peaks in Figure 3B were deconvoluted from the C 1s spectra of the composites, assigned to the C=C sp<sup>2</sup> shakes up at 284.8 eV, C-O at 286.2 eV and C=O at 288.0 eV<sup>[54]</sup>.

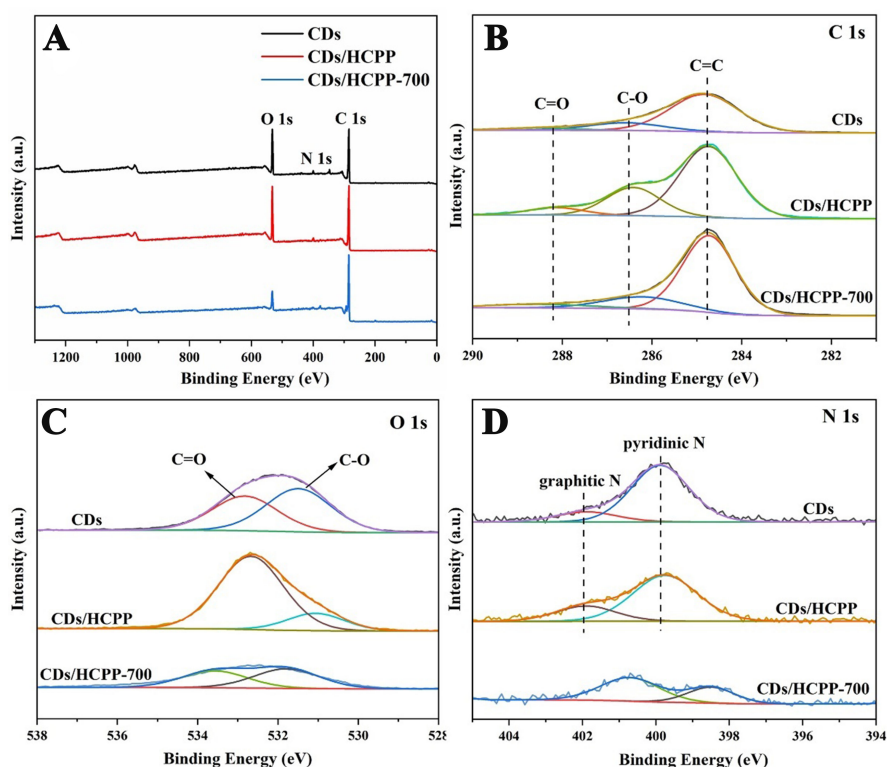


**Figure 1.** Schematic illustration of the synthesis route of samples. PP: Pomelo peel; CPP: carbonized PP; CDs: carbon dots.



**Figure 2.** XRD patterns of PP, CDs, CDs/HCPP and CDs/HCPP-700. CDs/HCPP: Carbon dots incorporated in hydrochar; CDs: carbon dots; PP: pomelo peel; XRD: X-ray diffraction.

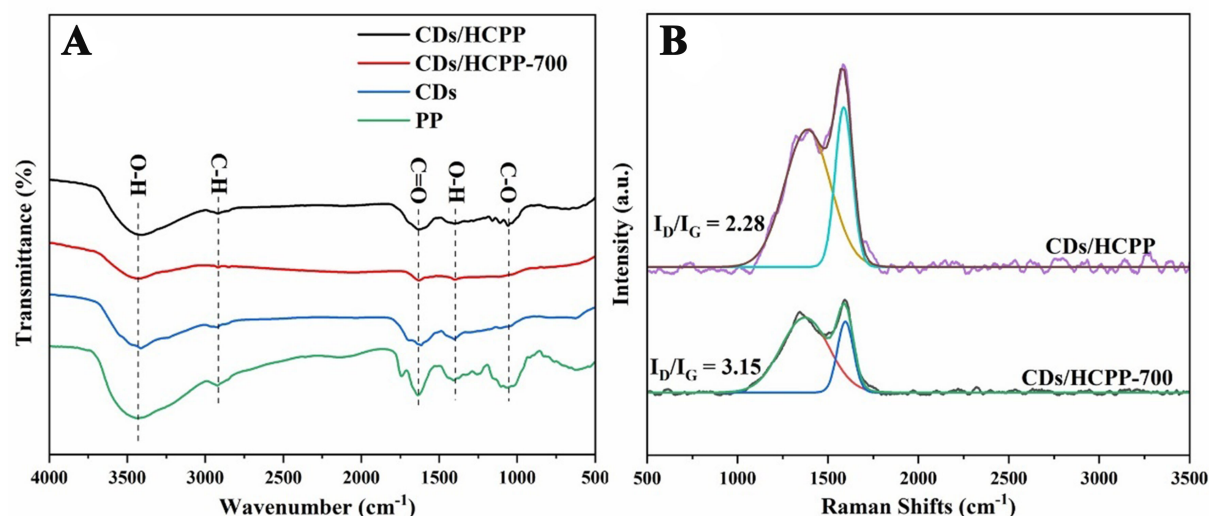
The XPS spectra of high-resolution O 1s show that the surface of the hydrochar is enriched with varying amounts of oxygen functional groups, including the C–O group at 531.9 eV and the C=O group at 533.6 eV [Figure 3C]. This phenomenon indicates that organic carbon binds to most of the oxygen<sup>[55]</sup>. Two typical nitrogen components in both CDs and CDs/HCPP are observed at 399.8 eV [pyridinic N (–N–)] and 401.9 eV [graphitic N (–NH–)] in the N1s spectra [Figure 3D]<sup>[56]</sup>. In contrast, a nitrogen component at about 400.3 eV was assigned to pyrrolic N in CPP [Supplementary Figure 3].



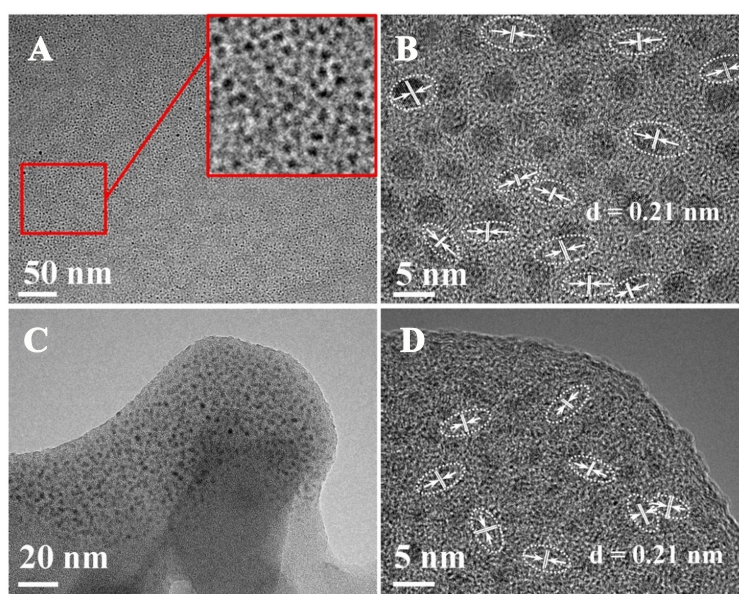
**Figure 3.** XPS spectra of as-prepared materials (A) survey; (B) C 1s; (C) O 1s; (D) N 1s. CDs: Carbon dots; CDs/HCPP: carbon dots incorporated in hydrochar; XPS: X-ray photoelectron spectroscopy.

Figure 4A shows the FT-IR spectra of PP, CDs, CDs/HCPP, and CDs/HCPP-700. In the spectrum of PP (black curve), the peak at  $3,439\text{ cm}^{-1}$  corresponds to the stretching vibration of O–H, the peak at  $2,930\text{ cm}^{-1}$  corresponds to the stretching vibration of C–H, and the peak at  $1,068\text{ cm}^{-1}$  corresponds to the stretching vibration of C–O. The absorption band corresponding to the stretching vibration of C=O is observed at  $1,708\text{ cm}^{-1}$ . Additionally, the stretching vibrations of C–H bonds in the aromatic rings are observed in the absorption band located at  $2,930\text{ cm}^{-1}$ [57]. Similar functional groups were observed in CPP [Supplementary Figure 4]. The degree of functionalization of the test samples can be evaluated in the Raman spectra displayed in Supplementary Figure 5. Figure 4B shows the presence of in-plane defects in disordered carbon leads to the characteristic D band centered at  $1,356\text{ cm}^{-1}$  in all spectra, while the graphite layers correspond to the adjacent G band centered at  $1,584\text{ cm}^{-1}$ [58]. The range of defect density can be elucidated by calculating the relative intensity ( $I_D/I_G$ ) of the two modes[58,59]. The incorporation of functional groups leads to fewer defects and less disorder. Therefore, the  $I_D/I_G$  of CDs/HCPP (2.28) is lower than that of CDs/HCPP-700. As shown in Supplementary Figure 6, Measuring the mass degradation curve under atmospheric conditions to simulate real-world scenarios is due to the inherent water evaporation, resulting in partial mass degradation of the sample below  $100\text{ }^{\circ}\text{C}$ . Decomposition up to the upper limit temperature of  $200\text{ }^{\circ}\text{C}$  was not observed. Based on the above results, CDs/HCPP exhibits significant stability in terms of repeatability and thermal performance, thus demonstrating its practical applicability.

Figure 5 is the TEM result of CDs and C. Figure 5A and C shows that the CDs were nearly monodisperse and almost spherical. The lattice structure of CDs and CDs/HCPP with spacing estimated to be  $0.21\text{ nm}$ , which corresponds to the lattice spacing of graphene (1 0 1) crystal plane.

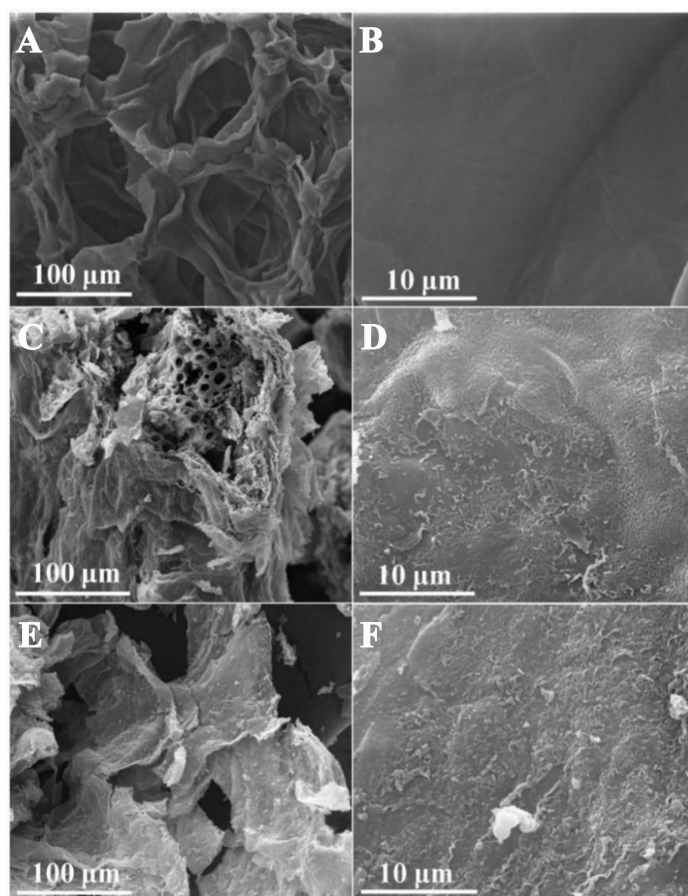


**Figure 4.** FT-IR spectra a. and Raman spectrum b. of the as-prepared materials. CD<sub>s</sub>/HCPP: Carbon dots incorporated in hydrochar; CD<sub>s</sub>: carbon dots; PP: pomelo peel; FT-IR: Fourier transform infrared spectroscopy.



**Figure 5.** TEM and HRTEM image of (A and B) CDs, (C and D) CD<sub>s</sub>/HCPP. TEM: Transmission electron microscopy; HRTEM: high-resolution transmission electron microscopy; CD<sub>s</sub>: carbon dots; CD<sub>s</sub>/HCPP: carbon dots incorporated in hydrochar.

Moreover, the SEM images were utilized to examine the microstructures of PP before and after modification<sup>[60]</sup>. A three-dimensionally (3D) reticulated macroporous architecture was observed. It revealed that PP had a net-like structure made up of interconnected macropores with diameters around 100–200  $\mu\text{m}$  [Figure 6A]. In addition, the hollow structures and smooth morphology are characteristic features of the surface of PP [Figure 6B]. Upon subjecting PP to hydrothermal treatment, a remarkable metamorphosis transpired. The once uniform and smooth surface gave way to an irregular and porous structure [Figure 6C]. The evolution continued as the surface of CD<sub>s</sub>/HCPP grew rougher, with the emergence of intricate crack and pore structures [Figure 6D–F]. This transmutation can be attributed to the aqueous environment of hydrothermal carbonization, where water assumes the role of a polar organic solvent,



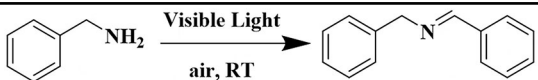
**Figure 6.** SEM images of (A and B) PP, (C and D) CDs/HCPP, (E and F) CDs/HCPP-700. SEM: Scanning electron microscopy; CDs/HCPP: carbon dots incorporated in hydrochar.

facilitating the harmonious blending of small organic compounds with the water solvent<sup>[61]</sup>. This synergy results in the enhanced dissolution of small organic compounds from the feedstocks, giving rise to a porous and more loosely structured foundation for CDs/HCPP<sup>[62]</sup>. However, the pore structure of CDs/HCPP-700 collapses, and the number of pores is significantly reduced after pyrolysis, which is consistent with BET surface area. Similar changes were observed in CPP-700 [Supplementary Figure 7].

### Photocatalytic oxidative coupling of amines

The preliminary selection of 0.02 mmol-scale benzylamine as a substrate is aimed at examining the catalytic activity and efficiency of grapefruit peel-derived catalysts in the amine oxidation coupling process. Before initiating the photocatalytic reaction, it is necessary to achieve adsorption/desorption equilibrium in the dark. Therefore, the suspension needs to be stirred for one hour without light exposure. All controlled trials are shown in Table 1. In the absence of catalysis or a light source, minimal conversion and selectivity are observed, thus confirming that the oxidation of benzylamine is indeed a reaction driven by visible light (Table 1, entries 1,4). Additionally, we corroborated the involvement of ambient air as the oxidizing agent in this reaction. After purging the reaction atmosphere with nitrogen gas to make it inert, it was observed that only a small fraction of benzylamine (2.2%) underwent oxidation. Typically, solvents play a significant role in organic reactions. Hence, the photocatalytic reaction was investigated in various solvents (Table 1, entries 10-15), revealing acetonitrile was the most efficient solvent for oxidative coupling.

**Table 1. Catalytic performance of various catalysts in the photo-oxidation of benzylamine<sup>a</sup>**



Entry	Catalyst	Solvent	Time/h	Conv./% <sup>d</sup>	Sel./% <sup>d</sup>
1	None	CH <sub>3</sub> CN	6	-	-
2	PP	CH <sub>3</sub> CN	6	< 1	-
3	CDs	CH <sub>3</sub> CN	6	87	99
4 <sup>b</sup>	CDs/HCPP	CH <sub>3</sub> CN	6	-	-
5 <sup>c</sup>	CDs/HCPP	CH <sub>3</sub> CN	6	2.2	99
6	CDs/HCPP	CH <sub>3</sub> CN	6	99	99
7	CPP	CH <sub>3</sub> CN	6	19	99
8	CDs/ CPP	CH <sub>3</sub> CN	6	40	99
9	CDs/HCPP-700	CH <sub>3</sub> CN	6	18	99
10	CDs/HCPP	DMSO	6	50	99
11	CDs/HCPP	CH <sub>2</sub> Cl <sub>2</sub>	6	68	99
12	CDs/HCPP	CHCl <sub>3</sub>	6	86	96
13	CDs/HCPP	EtOAc	6	93	99
14	CDs/HCPP	DMF	6	95	93
15	CDs/HCPP	CH <sub>3</sub> OH	6	96	98

<sup>a</sup>Standard reaction conditions: 20 mg of catalyst, 0.2 mmol of benzylamine, 5 mL of CH<sub>3</sub>CN, Air, 10 W LED, 25 °C, 8 h; <sup>b</sup>Without light irradiation; <sup>c</sup>Under N<sub>2</sub> atmosphere; <sup>d</sup>The conversion and selectivity for imines were assessed using GC. PP: Pomelo peel; CDs: carbon dots; CDs/HCPP: carbon dots incorporated in hydrochar; CPP: carbonized PP; DMSO: dimethyl sulfoxide; DMF: dimethylformamide; LED: light emitting diode; GC: gas chromatography.

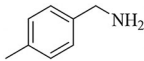
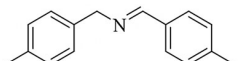
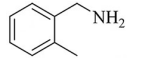
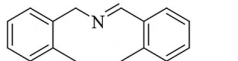
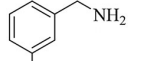
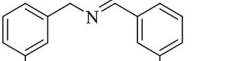
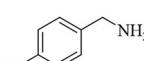
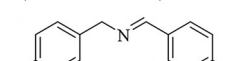
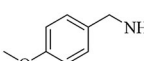
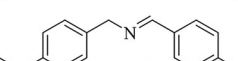
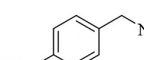
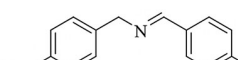
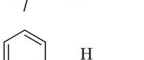
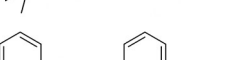
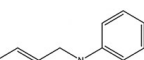
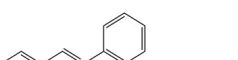

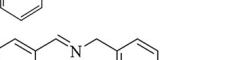
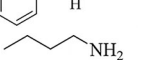
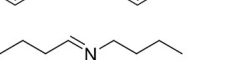
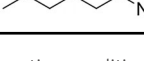
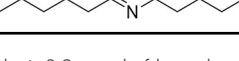
To further investigate the photocatalytic oxidation coupling reactions of different amines, HCPP was employed, as outlined in Table 2. Overall, the substituents of benzylamine have been proven to be suitable substrates for the reaction. In addition, it was observed that the reaction sensitivity varied based on the steric hindrance of the substituents on the phenyl ring. Para-substituted amines exhibit higher activity compared to meta- and ortho-substituted isomers (Table 2, entries 1-3). Efforts were undertaken to oxidize challenging aliphatic amines, and although high conversion rates were achieved, a lower selectivity of the product was observed (Table 2, entries 10-11) owing to the presence of inactive  $\alpha$ -hydrogens in the amine.

Supplementary Table 3 summarizes different carbon materials for photocatalytic oxidation of benzylamine. Actually, the reported reaction system for efficient benzylamine conversion still needs to be implemented by using high-pressure oxygen as the oxidant (entries 1-5)<sup>[2,20,42,63,64]</sup>, higher reaction temperature (entries 2, 5)<sup>[20,63]</sup> and longer reaction time (entries 1-4)<sup>[2,19,42,63]</sup>. The research on metal-free catalyst oxidation under visible light shows that straight-chain compounds, such as butylamine and aliphatic amines (entries 10, 11), are difficult to oxidize<sup>[65,66]</sup>. By incorporating the metal element Bi<sup>[67]</sup>, which can achieve higher selectivity, the conversion rate is only 51.4%. In contrast, the catalyst studied in this paper can oxidize straight-chain compounds under visible light and metal-free doping conditions with a conversion rate as high as 99%. Significantly, the novel PP-derived CDs/HCPP provided by this work was the efficient visible light photocatalysts, which shows good photocatalytic activity at room temperature, and the application is relatively broad.

### Recyclability test

As shown in Figure 7, the main focus of the study was the recyclability of photoactive CDs/HCPP in the oxidative coupling reaction of benzylamine under visible-light irradiation. After each cycle of the reaction, both the conversion and the selectivity of CDs/HCPP still retained more than 95.0% efficacy even after

**Table 2. The selective oxidation of different aromatic amines with CDs/HCPP as catalyst<sup>a</sup>**

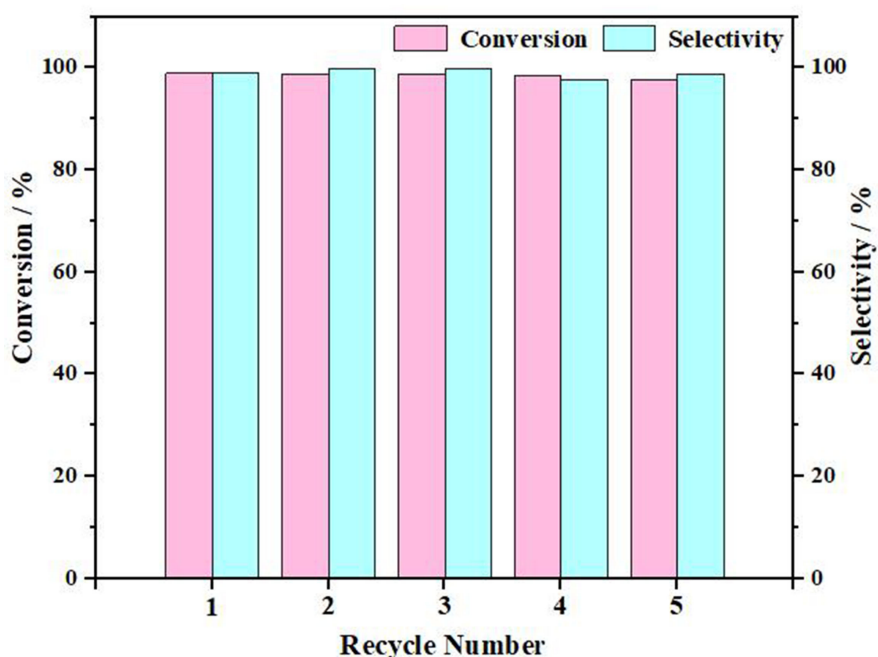
Entry	Substrate	Product	Time/h	Conv./% <sup>b</sup>	Sel./% <sup>b</sup>
1			6	85	95
2			6	88	94
3			6	95	95
4			6	90	93
5			6	58	64
6			6	86	92
7			6	80	57
8			6	84	94
9			6	94	93
10			6	99	45
11			6	99	38

<sup>a</sup>Standard reaction conditions: 20 mg of catalyst, 0.2 mmol of benzylamine, 5 mL of CH<sub>3</sub>CN, Air, 10 W LED, 25 °C, 8 h; <sup>b</sup>The conversion and selectivity for imines were assessed using GC. CDs/HCPP: Carbon dots incorporated in hydrochar; LED: light emitting diode; GC: gas chromatography.

being reused for five cycles. To validate the structural stability of the catalysts, the utilized catalyst was analyzed by XRD, with the results presented in [Supplementary Figure 8](#). The XRD patterns of the fresh and used CDs/HCPP were similar, indicating no phase changes following the reaction. This suggests that the CDs/HCPP was both recyclable and stable throughout the photocatalytic oxidation process.

### Plausible mechanism of photocatalytic oxidation of amines

As shown in [Figure 8A](#), CDs/HCPP displays complete absorption in the visible region compared to PP, indicating its potential as an intriguing candidate for visible-induced photocatalytic reactions. The absorption intensity of CDs/HCPP-700 and CPP [[Figure 8](#), [Supplementary Figure 9](#)] significantly increases in the full wavelength range, which directly proves the creation of graphite domains. Typically, photoluminescence (PL) intensity is associated with the recombination of electrons and holes. As shown in [Figure 8B](#), the PL of CDs/HCPP, CDs, and CDs/HCPP-700 materials is excited at 240 nm and emits around 290 and 390 nm. The PL intensity of CDs/HCPP is lower than that of CDs/HCPP-700 materials. Therefore, CDs/HCPP materials can effectively suppress electron recombination, possibly due to the introduction of CDs, further enhancing photocatalytic activity. CDs/HCPP exhibits the lowest PL intensity and highest benzylamine photocatalytic oxidation coupling yield, consistent with experimental results.



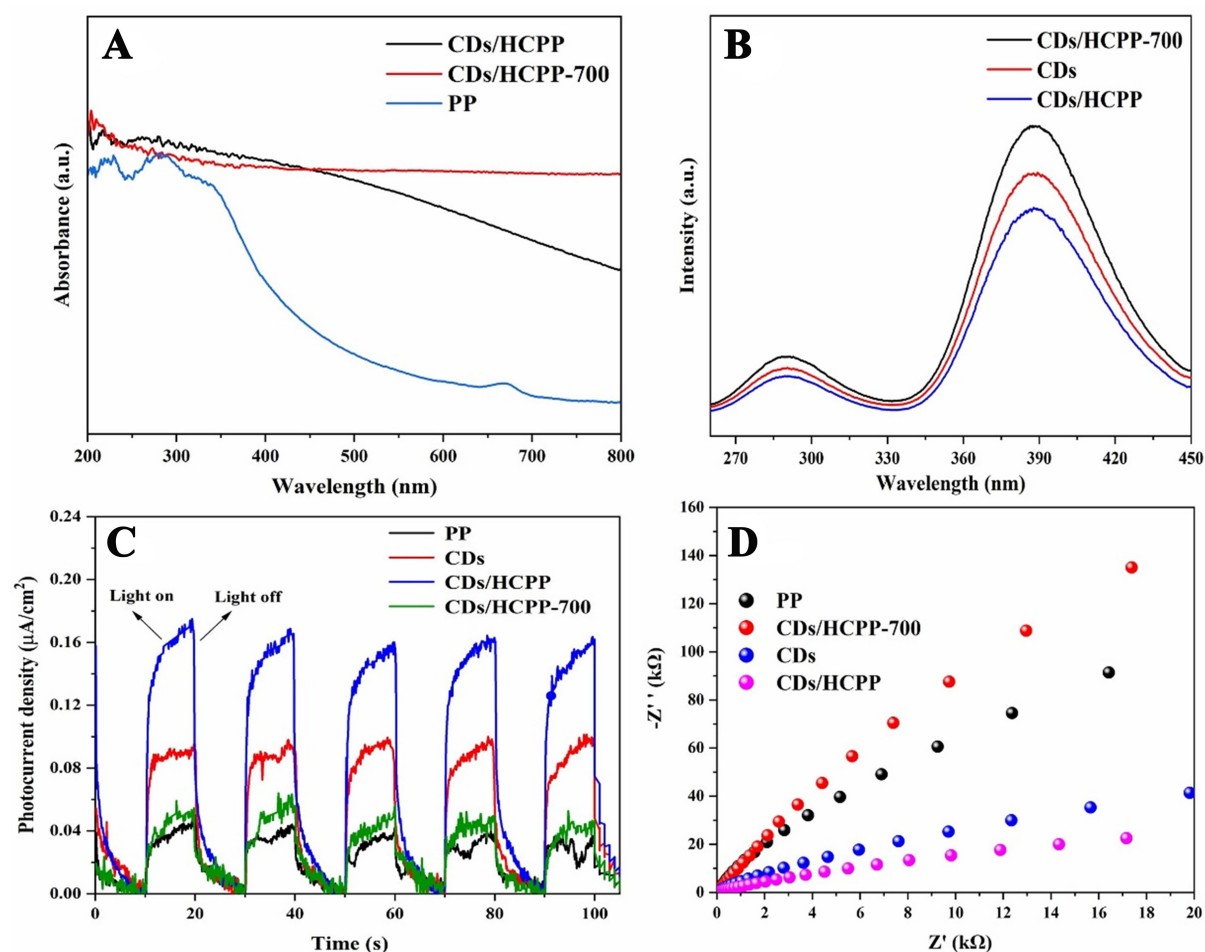
**Figure 7.** Recyclability performance of CDs/HCPP and XRD pattern of CDs/HCPP before and after reaction. CDs/HCPP: Carbon dots incorporated in hydrochar; XRD: X-ray diffraction.

**Supplementary Figure 10** is an ultraviolet-visible (UV-vis) absorption spectrum illustrating the absorption characteristics of the CD solution. This solution shows strong absorption in the range of 200 to 300 nm. Two shoulder peaks at 260 and 300 nm were observed, which were attributed to the  $\pi \rightarrow \pi^*$  transition of C=C and the  $n \rightarrow \pi^*$  transition of C=O, respectively<sup>[68]</sup>.

The aqueous solution is yellow and transparent in daylight but changes to intense blue under UV excitation (at 365 nm) (insets, **Figure 8B**).

The efficiency of charge carrier transfer and recombination in the prepared samples is elucidated through PL emission spectra [**Figure 8B**]. CDs with surface oxygen-containing functional groups and hollow microspheres can enhance the separation of electron-hole pairs, thereby inhibiting the recombination of charge carriers, resulting in a significant reduction in PL signal observed in the hydrochar samples. For the CD solution, varying the excitation wavelength from 400 to 500 nm causes the emission peak to be gradually red-shifted [**Supplementary Figure 11**]. The excitation-dependent emission is an inherent characteristic of the carbon particles<sup>[69]</sup>.

The photoresponse characteristics and charge carrier transfer ability of the hydrogenated carbon samples can be measured through photocurrent response measurements, and electrical impedance spectroscopy (EIS) was conducted. As shown in **Figure 8C**, the photocurrent density of the as-prepared samples is consistent and repeatable under each irradiation, exhibiting a gradual decline over time. Photocurrent intensity of CDs/HCPP is the highest, as nearly four times stronger than that of CDs/HCPP-700 and PP and two times stronger than that of CDs; this suggests that the separation of electron-hole pairs is due to charge transfer at the interface, leading to excellent photocatalytic performance. Meanwhile, the EIS Nyquist measurement was also researched, and **Figure 8D** shows the results. The smaller arc observed in an EIS Nyquist plot means the lower charge transfer resistance ( $R_{ct}$ ). Compared with the minimum arc, the

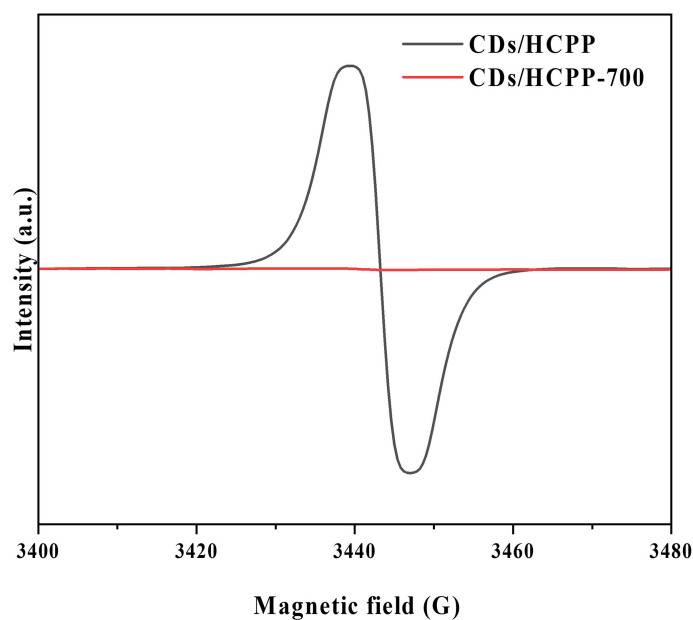


**Figure 8.** UV-vis spectra (A) PL spectra, (B) transient photocurrent response, (C) and (D) EIS Nyquist plots of the as-prepared samples. CD/HCPP: Carbon dots incorporated in hydrochar; PP: pomelo peel; CDs: carbon dots; UV-vis: ultraviolet-visible; PL: photoluminescence; EIS: electrical impedance spectroscopy.

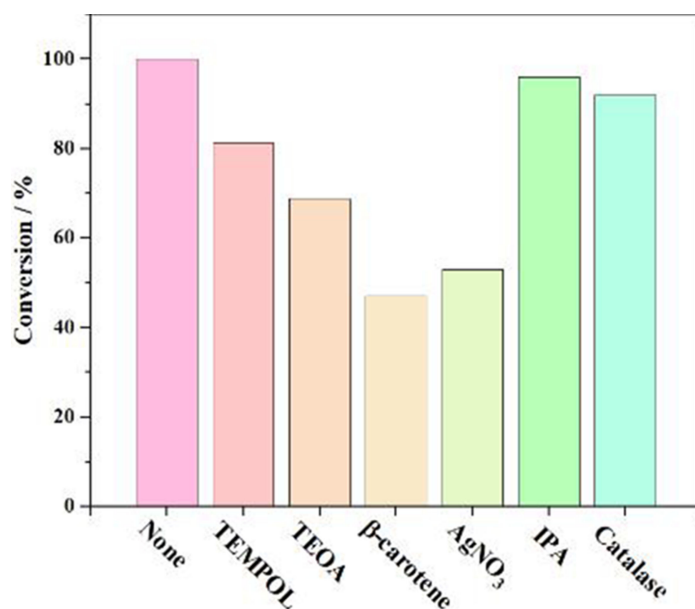
electrode of CD/HCPP demonstrates a smaller arc radius compared with those of CDs, CD/HCPP-700, and PP, and this suggests that CD/HCPP facilitates faster charge transfer at the interface. Furthermore, the equivalent circuit diagram [Supplementary Figure 12] of CD/HCPP was obtained through fitting, along with a  $R_{ct}$  value of 10,918  $\Omega$  and a series resistance ( $R_s$ ) value of 148.66  $\Omega$ .

Therefore, to enhance photocatalytic activity and promote the separation of photogenerated charges, the incorporation of CDs is advisable during the amine oxidation coupling process. This viewpoint is supported by all the aforementioned results.

As observed in the EPR spectra in Figure 9, both morphologies exhibit a signal at  $g = \sim 2.002$ , attributed to oxygen vacancies (OVs)<sup>[67,70]</sup>. The CD/HCPP sample displays a significantly stronger intensity compared to CD/HCPP-700, indicating a higher quantity of OVs in the former. Previous reports indicate that to enhance the activity of photocatalysts and impede the recombination of photogenerated electron-hole pairs, it is necessary to increase the number of OVs serving as electron-trapped sites<sup>[67,71]</sup>. The OVs have been reported to promote the activation of molecular oxygen<sup>[72]</sup> and the generation of ROS<sup>[73]</sup>, which may also facilitate the oxidative transformation of benzylamine in this study.

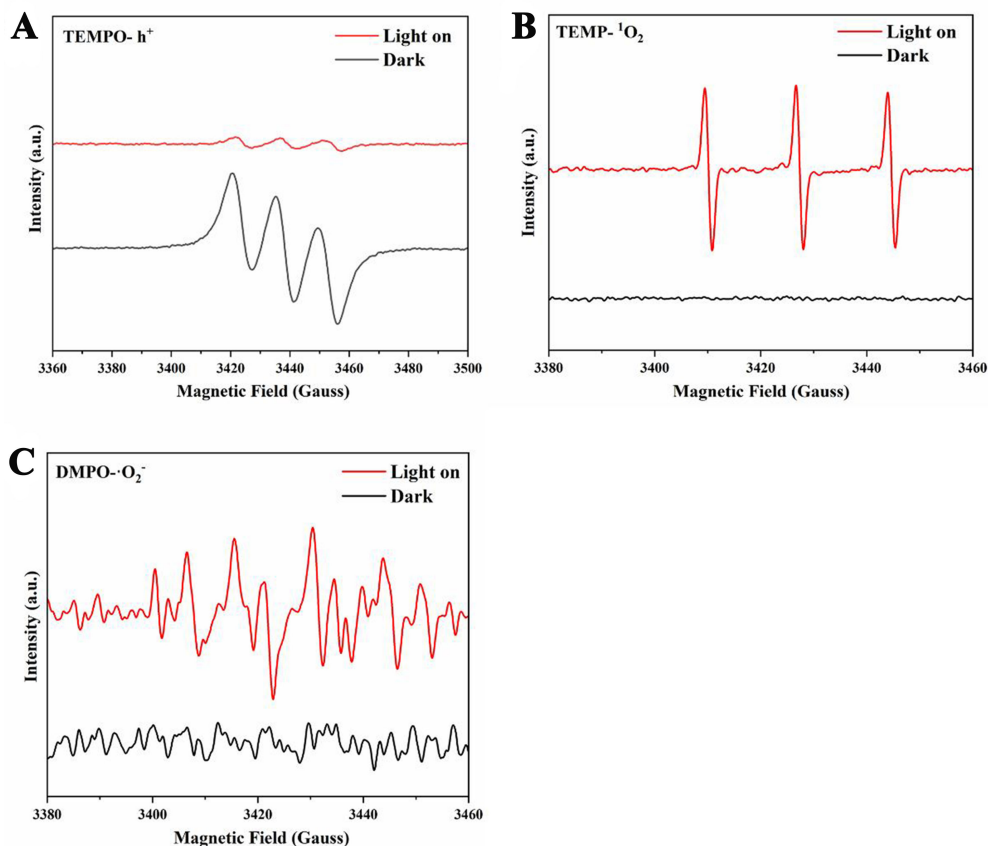


**Figure 9.** The EPR spectra of CDs/HCPP and CDs/HCPP-700 particles. CDs/HCPP: Carbon dots incorporated in hydrochar; EPR: electron paramagnetic resonance.



**Figure 10.** Photocatalytic oxidative coupling properties of CDs/HCPP using different radical scavengers. TEMPOL: 2,2,6,6-tetramethyl-4-piperidinol 1-oxyl; TEOA: triethanolamine; IPA: isopropyl alcohol; CDs/HCPP: carbon dots incorporated in hydrochar.

Control experiments were conducted to further understand the role of photocatalytic free radicals in these oxidation-reduction reactions. Figure 10 demonstrates the impact of various radical scavengers on the photocatalytic oxidation of benzylamine under visible light. Compared to other scavengers, notable reductions in the activities for the photocatalysis were observed when  $\beta$ -carotene (scavenger for singlet oxygen radicals,  $^1\text{O}_2$ ) was added into the photocatalysis system.

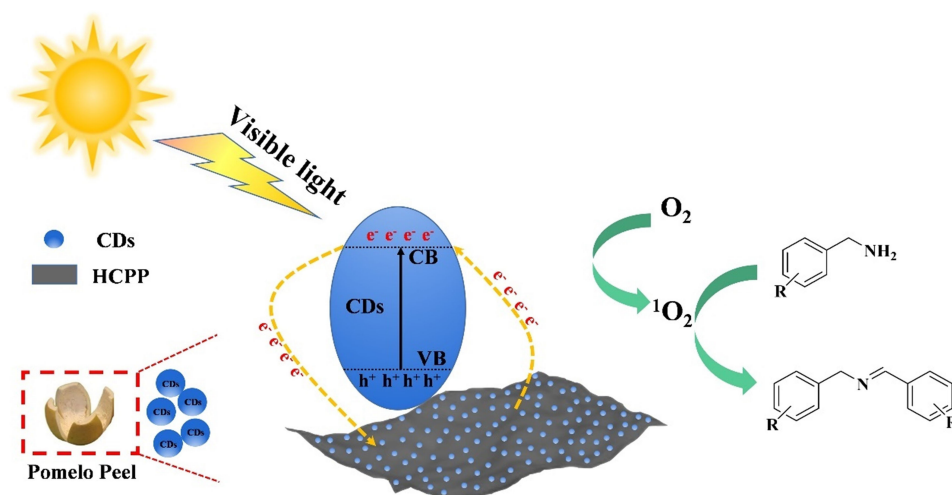


**Figure 11.** (A) The EPR spectra by adding TEMPO to capture  $h^+$ ; (B) the EPR spectra by adding TEMP to capture  $^1O_2$ ; and (C) the EPR spectra by adding DMPO to capture  $\cdot O_2^-$ . TEMPO: 2,2,6,6- tetramethyl-4-piperidinol 1-oxyl; TEMP: 2,2,6,6- tetramethyl-4-piperidinol; DMPO: 5,5-dimethyl-1-pyrroline N-oxide; EPR: electron paramagnetic resonance.

This outcome indicates that the ( $^1O_2$ ) radical formed is the primary active oxidation species involved in the selective oxidation of amines to imines. Slight decreases in the photo-oxidation activities were noted when  $AgNO_3$  (quenching electrons), triethanolamine (TEOA) (quenching holes) and 4-hydroxy-2,2,6,6-tetramethylpiperidine-1-oxyl (TEMPOL, quenching  $\cdot O_2^-$ ) were utilized as quenchers in the photocatalytic reaction. Indeed, the formation of photo-initiated the  $h^+$ ,  $^1O_2$  and  $O_2^-$  radicals over CDs/HCPP during the catalytic reaction was directly confirmed by Figure 11A-C.

Based on the analysis and literature reports, a plausible mechanism for the photocatalytic oxidative coupling of amines by the material can be elucidated in Figure 12. CDs excite electrons from the valence band (VB) to the conduction band (CB) under visible light irradiation, which forms photogenerated electron-hole pairs. As a key participant in the photo-oxidation process, active oxygen species ( $^1O_2$ ) are formed since the molecular  $O_2$  accepts the photoinduced electron transfer.

According to the reported literature, we also anticipate the formation of other side products, such as hydrogen peroxide ( $H_2O_2$ ) and ammonia ( $NH_3$ ), in the reaction. After the completion of the reaction, to verify the presence of ammonia, concentrated hydrochloric acid drops were added into the reaction vial. The dense white fumes observed confirmed the presence of ammonia<sup>[74]</sup>. A standard spectrophotometric method was used to identify the in situ generated  $H_2O_2$ . The appearance of two absorption maxima occurring at 510 and 552 nm [Supplementary Figure 13] proved the existence of  $H_2O_2$  in the reaction<sup>[75]</sup>.



**Figure 12.** Proposed mechanism for the oxidative coupling of amines in the presence of CDs/HCPP catalyst CDs/HCPP. CDs: Carbon dots; HCPP: hydrochar derived from PP; CB: conduction band; VB: valence band; CDs/HCPP: carbon dots incorporated in hydrochar.

Based on the above results and ultraperformance liquid chromatography (UPLC)-MS results shown in [Supplementary Figures 14 and 15](#), a mechanistic pathway for the photocatalytic oxidative coupling of benzylamine over CDs/HCPP was introduced. Upon irradiation, benzylamine M1 first undergoes alkene reaction with singlet oxygen (path I) to form peroxide M2, and then releases hydrogen peroxide, which takes the recovery of aromaticity as the driving force to generate imine intermediate M3, which reacts with water to form benzaldehyde M4.

The coupling product M5 was formed by M4 (Path A) or M3 (Path B) reacting with the free amine<sup>[63]</sup>. Peroxide complex M2 can be formed by benzylamine M1 reacting with oxygen (path II), followed by the formation of imine intermediate M3 after the release of hydrogen peroxide. Oxygen insertion may also involve a free radical pathway, where the formation of benzyl radical occurs due to the abstraction of  $\alpha$ -hydrogen of M1 by oxygen. The benzyl radical then reacts with oxygen to form the peroxide complex M2 (path III)<sup>[76]</sup>. Hydrogen peroxide may be a possible oxidant in the oxidation reaction, and a control experiment with catalase acting as the scavenger of hydrogen peroxide was performed under standard conditions [\[Figures 5-12\]](#). After the addition of catalase [\[Figure 10\]](#), the conversion of CDs/HCPP was still over 90%, which indicated that the  $\text{H}_2\text{O}_2$  formed in the reaction did not play a leading role in the photocatalytic oxidative coupling of benzylamine.

## CONCLUSIONS

In this work, a facile and effective one-pot technique has been proposed to directly fabricate blue luminescent CDs and CDs/HCPP from fresh PP. CDs/HCPP exhibited the highest photocurrent intensity, nearly four times stronger than that of CDs/HCPP-700 and PP, and twice as strong as that of CDs alone. Significantly, research on metal-free catalyst oxidation under visible light has demonstrated the difficulty of oxidizing straight-chain compounds, such as butylamine and aliphatic amines. Incorporating the metal element Bi can achieve higher selectivity; however, the conversion rate remains at only 51.4%. In contrast, the catalyst studied in this paper achieves an impressive 99% conversion rate for oxidizing straight-chain compounds under visible light and metal-free doping conditions. This performance was nearly 5.5 times that of CPP without CDs and 1.14 times that of CDs alone, outperforming other counterpart catalysts and reported photocatalytic systems. After experimenting with various solvents, acetonitrile exhibited the best performance as a photocatalytic medium. The catalyst also demonstrated excellent photocatalytic activity

and recyclability in the aerobic oxidative coupling reactions of different amines. Through in-depth research, the mechanism of the CDs/HCPP photocatalyzed oxidative coupling of amines has been elucidated. To our knowledge, the use of CDs/HCPP as photocatalysts for light-driven organic synthesis has been reported for the first time. In this research context, other reactions driven by visible light can also be attempted using CD/HCPP-based photocatalysts.

## DECLARATIONS

### Authors' contributions

Designed the experiments, conducted characterization, analyzed data, interpreted results, drew the pictures, and wrote the manuscript: Cao X, Zhao Y

Synthesized samples: Leng J, Bai X, Qu Y

Contributed to helpful discussions and provided material support: Wang J, Chen D, Jiang L

Directed and supervised the project and revised the manuscript: Wang J

### Availability of data and materials

Not applicable.

### Financial support and sponsorship

This work was supported by the National Natural Science Foundation of China (22062026), the Yunling Scholar (YNWR-YLXZ-2019-002), the Department of Ecology and Environment of Yunnan Province [YNDM-2023-0123 (A)], and the Program for Innovation Team of Yunnan Province and the Key Laboratory of Advanced Materials for Wastewater Treatment of Kunming (2110304). The authors thank the Advanced Analysis and Measurement Center of Yunnan University for the sample testing service.

### Conflicts of interest

All authors declared that there are no conflicts of interest.

### Ethical approval and consent to participate

Not applicable.

### Consent for publication

Not applicable.

### Copyright

© The Author(s) 2024.

## REFERENCES

1. Garg R, Mondal S, Sahoo L, Vinod CP, Gautam UK. Nanocrystalline Ag<sub>3</sub>PO<sub>4</sub> for sunlight- and ambient air-driven oxidation of amines: high photocatalytic efficiency and a facile catalyst regeneration strategy. *ACS Appl Mater Interfaces* 2020;12:29324-34. DOI PubMed
2. Ye J, Ni K, Liu J, Chen G, Ikram M, Zhu Y. Oxygen-rich carbon quantum dots as catalysts for selective oxidation of amines and alcohols. *ChemCatChem* 2018;10:259-65. DOI
3. Wang Z, Lang X. Visible light photocatalysis of dye-sensitized TiO<sub>2</sub>: the selective aerobic oxidation of amines to imines. *Appl Catal B Environ* 2018;224:404-9. DOI
4. Raza F, Park JH, Lee HR, Kim HI, Jeon SJ, Kim JH. Visible-light-driven oxidative coupling reactions of amines by photoactive WS<sub>2</sub> nanosheets. *ACS Catal* 2016;6:2754-9. DOI
5. Su F, Mathew SC, Möhlmann L, Antonietti M, Wang X, Blechert S. Aerobic oxidative coupling of amines by carbon nitride photocatalysis with visible light. *Angew Chem Int Ed Engl* 2011;50:657-60. DOI PubMed
6. Kumar A, Kumar P, Joshi C, et al. A [Fe(bpy)<sub>3</sub>]<sup>2+</sup> grafted graphitic carbon nitride hybrid for visible light assisted oxidative coupling of benzylamines under mild reaction conditions. *Green Chem* 2016;18:2514-21. DOI
7. Wei H, Guo Z, Liang X, Chen P, Liu H, Xing H. Selective photooxidation of amines and sulfides triggered by a superoxide radical

- using a novel visible-light-responsive metal-organic framework. *ACS Appl Mater Interfaces* 2019;11:3016-23. DOI PubMed
8. Kumar A, Sadanandhan AM, Jain SL. Silver doped reduced graphene oxide as a promising plasmonic photocatalyst for oxidative coupling of benzylamines under visible light irradiation. *New J Chem* 2019;43:9116-22. DOI
  9. Kumar R, Gleissner EH, Tiu EG, Yamakoshi Y. C70 as a photocatalyst for oxidation of secondary benzylamines to imines. *Org Lett* 2016;18:184-7. DOI PubMed
  10. Li H, Kang Z, Liu Y, Lee S. Carbon nanodots: synthesis, properties and applications. *J Mater Chem* 2012;22:24230. DOI
  11. Han M, Zhu S, Lu S, et al. Recent progress on the photocatalysis of carbon dots: classification, mechanism and applications. *Nano Today* 2018;19:201-18. DOI
  12. Bian J, Huang C, Wang L, Hung T, Daoud WA, Zhang R. Carbon dot loading and TiO<sub>2</sub> nanorod length dependence of photoelectrochemical properties in carbon dot/TiO<sub>2</sub> nanorod array nanocomposites. *ACS Appl Mater Interfaces* 2014;6:4883-90. DOI PubMed
  13. Zhang J, Xu J, Tao F. Interface modification of TiO<sub>2</sub> nanotubes by biomass-derived carbon quantum dots for enhanced photocatalytic reduction of CO<sub>2</sub>. *ACS Appl Energy Mater* 2021;4:13120-31. DOI
  14. Zhou D, Li D, Jing P, et al. Conquering aggregation-induced solid-state luminescence quenching of carbon dots through a carbon dots-triggered silica gelation process. *Chem Mater* 2017;29:1779-87. DOI
  15. Su J, Lu S, Hai J, et al. Confining carbon dots in porous wood: the singlet oxygen enhancement strategy for photothermal signal-amplified detection of Mn<sup>2+</sup>. *ACS Sustainable Chem Eng* 2020;8:17687-96. DOI
  16. Hu S, Zhou Y, Xue C, Yang J, Chang Q. A solid reaction towards in situ hybridization of carbon dots and conjugated polymers for enhanced light absorption and conversion. *Chem Commun* 2017;53:9426-9. DOI
  17. Huo P, Guan J, Zhou M, et al. Carbon quantum dots modified CdSe loaded reduced graphene oxide for enhancing photocatalytic activity. *J Ind Eng Chem* 2017;50:147-54. DOI
  18. Vattikuti SVP, Devarayapalli KC, Reddy Nallabala NK, Nguyen TN, Nguyen Dang N, Shim J. Onion-ring-like carbon and nitrogen from ZIF-8 on TiO<sub>2</sub>/Fe<sub>2</sub>O<sub>3</sub> nanostructure for overall electrochemical water splitting. *J Phys Chem Lett* 2021;12:5909-18. DOI PubMed
  19. Han Y, Huang H, Zhang H, et al. Carbon quantum dots with photoenhanced hydrogen-bond catalytic activity in aldol condensations. *ACS Catal* 2014;4:781-7. DOI
  20. Kumar A, Hamdi A, Coffinier Y, et al. Visible light assisted oxidative coupling of benzylamines using heterostructured nanocomposite photocatalyst. *J Photochem Photobiol A Chem* 2018;356:457-63. DOI
  21. Samanta S, Khilari S, Srivastava R. Stimulating the visible-light catalytic activity of Bi<sub>2</sub>MoO<sub>6</sub> nanoplates by embedding carbon dots for the efficient oxidation, cascade reaction, and photoelectrochemical O<sub>2</sub> evolution. *ACS Appl Nano Mater* 2018;1:426-41. DOI
  22. Wang Q, Li J, Tu X, et al. Single atomically anchored cobalt on carbon quantum dots as efficient photocatalysts for visible light-promoted oxidation reactions. *Chem Mater* 2020;32:734-43. DOI
  23. Pal A, Sk MP, Chattopadhyay A. Conducting carbon dot-polypyrrole nanocomposite for sensitive detection of picric acid. *ACS Appl Mater Interfaces* 2016;8:5758-62. DOI PubMed
  24. He Y, He J, Yu Z, et al. Double carbon dot assembled mesoporous aluminas: solid-state dual-emission photoluminescence and multifunctional applications. *J Mater Chem C* 2018;6:2495-501. DOI
  25. He Y, He J, Wang L, et al. Synthesis of double carbon dots co-doped mesoporous Al<sub>2</sub>O<sub>3</sub> for ratiometric fluorescent determination of oxygen. *Sens Actuators B: Chem* 2017;251:918-26. DOI
  26. Wang B, Wang H, Hu Y, Waterhouse GIN, Lu S. Carbon dot based multicolor electroluminescent LEDs with nearly 100% exciton utilization efficiency. *Nano Lett* 2023;23:8794-800. DOI
  27. Long C, Qing T, Fu Q, et al. Low-temperature rapid synthesis of high-stable carbon dots and its application in biochemical sensing. *Dyes Pigm* 2020;175:108184. DOI
  28. Aghamali A, Khosravi M, Hamishehkar H, Modirshahla N, Behnajady MA. Synthesis and characterization of high efficient photoluminescent sunlight driven photocatalyst of N-Carbon Quantum Dots. *J Lumin* 2018;201:265-74. DOI
  29. Pan D, Zhang J, Li Z, Wu C, Yan X, Wu M. Observation of pH-, solvent-, spin-, and excitation-dependent blue photoluminescence from carbon nanoparticles. *Chem Commun* 2010;46:3681-3. DOI
  30. Hou C, Liu K, Yu X, et al. Nitrogen-doped porous carbons synthesized with low-temperature sodium amide activation as metal-free catalysts for oxidative coupling of amines to imines. *J Mater Sci* 2021;56:16865-76. DOI
  31. Sun Y, Hou C, Cao X, Liu K. Facile synthesis of nitrogen-doped foam-like carbon materials from purslane stem as efficient metal-free catalysts for oxidative coupling of amines to imines. *J Mater Sci* 2021;56:6124-34. DOI
  32. Liu C, Li N, Peng L, Zhong W, Mao L, Yin D. Hydrothermal carbonization of renewable natural plants as superior metal-free catalysts for aerobic oxidative coupling of amines to imines. *ACS Sustainable Chem Eng* 2020;8:11404-12. DOI
  33. Chen T, Ye T, Zhu J, et al. Small-sized biomass-derived hydrothermal carbon with enriched oxygen groups quickens benzene hydroxylation to phenol with dioxygen. *Appl Catal A Gen* 2021;626:118356. DOI
  34. Titirici MM, Antonietti M. Chemistry and materials options of sustainable carbon materials made by hydrothermal carbonization. *Chem Soc Rev* 2010;39:103-16. DOI PubMed
  35. Chen N, Huang Y, Hou X, Ai Z, Zhang L. Photochemistry of hydrochar: reactive oxygen species generation and sulfadimidine degradation. *Environ Sci Technol* 2017;51:11278-87. DOI PubMed
  36. Ye Q, Huang Z, Wu P, et al. Promoting the photogeneration of hydrochar reactive oxygen species based on FeAl layered double

- hydroxide for diethyl phthalate degradation. *J Hazard Mater* 2020;388:122120. DOI
37. Sun X, Luo X, Zhang X, et al. Enhanced superoxide generation on defective surfaces for selective photooxidation. *J Am Chem Soc* 2019;141:3797-801. DOI
38. Wang H, Jiang S, Chen S, et al. Enhanced singlet oxygen generation in oxidized graphitic carbon nitride for organic synthesis. *Adv Mater* 2016;28:6940-5. DOI
39. Demir-cakan R, Makowski P, Antonietti M, Goettmann F, Titirici M. Hydrothermal synthesis of imidazole functionalized carbon spheres and their application in catalysis. *Catal Today* 2010;150:115-8. DOI
40. Titirici M, White RJ, Falco C, Sevilla M. Black perspectives for a green future: hydrothermal carbons for environment protection and energy storage. *Energy Environ Sci* 2012;5:6796. DOI
41. Zhao Z, Ge G, Li W, Guo X, Wang G. Modulating the microstructure and surface chemistry of carbocatalysts for oxidative and direct dehydrogenation: a review. *Chinese J Catal* 2016;37:644-70. DOI
42. Su F, Peng H, Yin H, et al. Biowaste-derived hydrochar microspheres: Realizing metal-free visible-light photocatalytic oxidation of amines. *J Catal* 2021;404:149-62. DOI
43. Wang W, Chen M. Catalytic degradation of sulfamethoxazole by peroxymonosulfate activation system composed of nitrogen-doped biochar from pomelo peel: Important roles of defects and nitrogen, and detoxification of intermediates. *J Colloid Interface Sci* 2022;613:57-70. DOI PubMed
44. Zhao S, Wang Y, Wang L, Jin Y. Preparation, characterization and catalytic application of hierarchically porous LaFeO<sub>3</sub> from a pomelo peel template. *Inorg Chem Front* 2017;4:994-1002. DOI
45. Ma R, Fakudze S, Shang Q, et al. Catalytic hydrothermal carbonization of pomelo peel for enhanced combustibility of coal/hydrochar blends and reduced CO<sub>2</sub> emission. *Fuel* 2021;304:121422. DOI
46. Sun H, Ni H, Chen F, Jiang Z, Huang G, Yang Y. Effect of oxygen and heating on aromas of pummelo (*Citrus maxima*) essential oil. *J Essent Oil Res* 2018;30:92-104. DOI
47. Zheng H, Sun Q, Li Y, Du Q. Biosorbents prepared from pomelo peel by hydrothermal technique and its adsorption properties for congo red. *Mater Res Express* 2020;7:045505. DOI
48. Tran HN, Tomul F, Thi Hoang Ha N, et al. Innovative spherical biochar for pharmaceutical removal from water: Insight into adsorption mechanism. *J Hazard Mater* 2020;394:122255. DOI
49. Huang R, Cao M, Guo H, Qi W, Su R, He Z. Enhanced ethanol production from pomelo peel waste by integrated hydrothermal treatment, multienzyme formulation, and fed-batch operation. *J Agric Food Chem* 2014;62:4643-51. DOI
50. Geng Y, Sun W, Ying P, et al. Bioinspired fractal design of waste biomass-derived solar - thermal materials for highly efficient solar evaporation. *Adv Funct Mater* 2021;31:2007648. DOI
51. Liu X, Mishra DD, Li Y, et al. Biomass-derived carbonaceous materials with multichannel waterways for solar-driven clean water and thermoelectric power generation. *ACS Sustainable Chem Eng* 2021;9:4571-82. DOI
52. Liu Q, Ma X, Zhao Y, et al. Facile synthesis of carbon dots incorporated carbonized pomelo peel by one-step method for enhanced solar evaporation. *Mater Today Sustain* 2023;23:100442. DOI
53. Ye H, Chen J, Hu Y, et al. One-pot synthesis of two-dimensional multilayered graphitic carbon nanosheets by low-temperature hydrothermal carbonization using the *in situ* formed copper as a template and catalyst. *Chem Commun* 2020;56:11645-8. DOI
54. Zhang P, O'Connor D, Wang Y, et al. A green biochar/iron oxide composite for methylene blue removal. *J Hazard Mater* 2020;384:121286. DOI
55. Ahmed MB, Zhou JL, Ngo HH, Johir MAH, Sornalingam K. Sorptive removal of phenolic endocrine disruptors by functionalized biochar: Competitive interaction mechanism, removal efficacy and application in wastewater. *Chem Eng J* 2018;335:801-11. DOI
56. Wang C, Jiang K, Wu Q, Wu J, Zhang C. Green synthesis of red-emitting carbon nanodots as a novel "turn-on" nanothermometer in living cells. *Chemistry* 2016;22:14475-9. DOI PubMed
57. Khan T, Kim H, Gupta A, Jamari SS, Jose R. Synthesis and characterization of carbon microspheres from rubber wood by hydrothermal carbonization. *J Chem Tech Biotech* 2019;94:1374-83. DOI
58. Fan W, Xia Y, Tjiu WW, Pallathadka PK, He C, Liu T. Nitrogen-doped graphene hollow nanospheres as novel electrode materials for supercapacitor applications. *J Power Sources* 2013;243:973-81. DOI
59. Cai X, Wang Q, Liu Y, et al. Hybrid of polyoxometalate-based ionic salt and N-doped carbon toward reductant-free aerobic hydroxylation of benzene to phenol. *ACS Sustain Chem Eng* 2016;4:4986-96. DOI
60. Ye P, Chen K, Yin Y, et al. A 3D-macroporous pomelo peel foam based on anti-shrinkage properties of MnOx for solar water purification. *J Environ Chem Eng* 2022;10:106890. DOI
61. Akiya N, Savage PE. Roles of water for chemical reactions in high-temperature water. *Chem Rev* 2002;102:2725-50. DOI PubMed
62. Fu M, Mo C, Li H, Zhang Y, Huang W, Wong MH. Comparison of physicochemical properties of biochars and hydrochars produced from food wastes. *J Clean Prod* 2019;236:117637. DOI
63. Khampuanbut A, Santalelat S, Pankiew A, et al. Visible-light-driven WO<sub>3</sub>/BiOBr heterojunction photocatalysts for oxidative coupling of amines to imines: Energy band alignment and mechanistic insight. *J Colloid Interface Sci* 2020;560:213-24. DOI PubMed
64. Zhang D, Han X, Dong T, Guo X, Song C, Zhao Z. Promoting effect of cyano groups attached on g-C<sub>3</sub>N<sub>4</sub> nanosheets towards molecular oxygen activation for visible light-driven aerobic coupling of amines to imines. *J Catal* 2018;366:237-44. DOI
65. Bai P, Tong X, Wan J, Gao Y, Xue S. Flower-like Bi<sub>2</sub>O<sub>3</sub>CO<sub>3</sub>-mediated selective oxidative coupling processes of amines under visible light irradiation. *J Catal* 2019;374:257-65. DOI

66. Zhang K, Huang F, Dong X, Xiong K, Lang X. Benzotrithiophene-based  $sp^2$  carbon-conjugated microporous polymers for green light-triggered oxidation of amines to imines. *Mater Today Chem* 2024;35:101879. DOI
67. Dissanayake D, Achola LA, Kerns P, et al. Aerobic oxidative coupling of amines to imines by mesoporous copper aluminum mixed metal oxides via generation of Reactive Oxygen Species (ROS). *Appl Catal B Environ* 2019;249:32-41. DOI
68. Liu L, Cai W, Dang C, et al. One-step vapor-phase assisted hydrothermal synthesis of functionalized carbons: effects of surface groups on their physicochemical properties and adsorption performance for Cr(VI). *Appl Surf Sci* 2020;528:146984. DOI
69. Zhang Y, Gonçalves H, da Silva JC, Geddes CD. Metal-enhanced photoluminescence from carbon nanodots. *Chem Commun* 2011;47:5313-5. DOI PubMed
70. Zeng X, Wan Y, Gong X, Xu Z. Additive dependent synthesis of bismuth oxybromide composites for photocatalytic removal of the antibacterial agent ciprofloxacin and mechanism insight. *RSC Adv* 2017;7:36269-78. DOI
71. Xue X, Chen R, Chen H, et al. Oxygen vacancy engineering promoted photocatalytic ammonia synthesis on ultrathin two-dimensional bismuth oxybromide nanosheets. *Nano Lett* 2018;18:7372-7. DOI
72. Li H, Shi J, Zhao K, Zhang L. Sustainable molecular oxygen activation with oxygen vacancies on the {001} facets of BiOCl nanosheets under solar light. *Nanoscale* 2014;6:14168-73. DOI
73. Wang H, Yong D, Chen S, et al. Correction to “oxygen-vacancy-mediated exciton dissociation in biobr for boosting charge-carrier-involved molecular oxygen activation”. *J Am Chem Soc* 2018;140:5320. DOI
74. Kumar I, Kumar R, Gupta SS, Sharma U.  $C_{70}$  fullerene catalyzed photoinduced aerobic oxidation of benzylamines to imines and aldehydes. *J Org Chem* 2021;86:6449-57. DOI PubMed
75. Xu C, Liu H, Li D, Su JH, Jiang HL. Direct evidence of charge separation in a metal-organic framework: efficient and selective photocatalytic oxidative coupling of amines via charge and energy transfer. *Chem Sci* 2018;9:3152-8. DOI PubMed PMC
76. Liu L, Zhang S, Fu X, Yan CH. Metal-free aerobic oxidative coupling of amines to imines. *Chem Commun* 2011;47:10148-50. DOI